

Expanding the homogeneous regime of deformation in bulk metallic glass by electromigration-induced rejuvenation

Qi Chen^{1,5}, Meng Zhang^{2,3,5}, Jiachang Gu², Quanliang Cao¹, Cheng Zhang², Xiaotao Han¹ [✉], Liang Li¹, Weihua Wang⁴ [✉] & Lin Liu² [✉]

The origin of plasticity in bulk metallic glasses (BMGs) is highly elusive due to their complicated amorphous atomic structures. Nonetheless, there is a general consensus that the homogeneous regime of deformation on the deformation map of BMGs is constrained by high temperature and low strain rate. Here we report an expanded homogeneous regime in a $Zr_{55}Cu_{30}Al_{10}Ni_5$ BMG, which is achieved by applying a pulsed electric current to the BMG specimen subjected to external loading. The BMG specimen exhibits homogeneous elongation and necking, rather than shear banding as it should without pulsed current. The results indicate that the pulsed current produces an additional effective “temperature increment” $\sim 0.15T_g$ (T_g , the glass transition temperature) apart from the Joule heating effect. This expanded homogeneous regime is attributed primarily to electromigration-induced dynamic rejuvenation which promotes homogeneously distributed deformation by enlarging the shear transformation zones. These findings could benefit understandings of plasticity in glassy materials.

¹Wuhan National High Magnetic Field Center and State Key Laboratory of Advanced Electromagnetic Engineering and Technology, Huazhong University of Science and Technology, 430074 Wuhan, China. ²State Key Lab for Materials Processing and Die & Mould Technology and School of Materials Science and Engineering, Huazhong University of Science and Technology, 430074 Wuhan, China. ³Institute of Advanced Wear & Corrosion Resistant and Functional Materials, Jinan University, 510632 Guangzhou, China. ⁴Institute of Physics, Chinese Academy of Sciences, 100190 Beijing, China. ⁵These authors contributed equally: Qi Chen, Meng Zhang. ✉email: xthan@mail.hust.edu.cn; whw@iphy.ac.cn; liu2000@mail.hust.edu.cn

Bulk metallic glasses (BMGs) feature their amorphous atomic structures which lack periodic crystalline lattice structure as well as crystalline defects, such as dislocations¹, twins², and grain boundaries³. Therefore, compared with crystalline alloys, the origin of plasticity in BMGs is much difficult to disclose⁴. As a convenient means of surveying the deformation mechanisms of materials, the deformation map initially developed for crystalline materials^{5,6} was also established for BMGs^{7–9}. Based on the deformation map in temperature–strain rate space⁸, the deformation of BMG could be divided into an inhomogeneous regime and a homogeneous regime. Near room temperature, the plastic deformation of BMG¹⁰ generally falls in the inhomogeneous regime via the formation of extremely localized shear bands¹¹. These shear bands nucleate through the self-assembly¹² of the elementary deformation units in BMGs called shear transformation zones (STZs)¹³ propelled by the long-range interactions between STZs along the plane of maximum shear stress, and tend to develop into open cracks leading to fracture¹⁴. While at temperatures above $\sim 0.8 T_g$ (T_g is the glass transition temperature) and at low enough strain rates, the plastic deformation of BMG usually follows the homogeneous mode¹⁵. This is because that the increased atomic mobility at elevated temperatures relaxes the long-range interactions between STZs rapidly enough, thus prevents the self-assembly of STZs into shear bands¹², i.e. suppresses shear banding. The “temperature-strain rate” boundaries separating the inhomogeneous and homogeneous regimes of deformation for bulk BMG specimens ever reported in the past decades indicate that, in the vicinity of T_g , the critical strain rate ($\dot{\epsilon}_c$) and the normalized temperature (T/T_g) roughly follow an empirical relation: $\lg \dot{\epsilon}_c \approx 22(T/T_g) - 25$ (see Supplementary Fig. 1), e.g. at $0.8 T_g$, $\dot{\epsilon}_c$ is estimated to be $\sim 10^{-7} \text{ s}^{-1}$; while at $0.95 T_g$, $\dot{\epsilon}_c$ increases rapidly to $\sim 10^{-4} \text{ s}^{-1}$. Therefore, although the atomistic mechanisms of plastic deformation in BMGs remain under debate, there is a general consensus that the homogeneous regime is constrained by high temperature and low strain rate, as having been well established in different theoretical models^{16–18}. On this basis, somehow could one alter the boundary of the homogeneous regime, the relevant observations would probably help to deepen current understandings on the plastic deformation of BMGs.

Here, we report an expanded homogeneous regime of deformation in a $\text{Zr}_{55}\text{Cu}_{30}\text{Al}_{10}\text{Ni}_5$ (Zr55) BMG via the application of pulsed electric current on the BMG specimen undergoing tensile deformation. The BMG displays a uniform plastic elongation followed by necking, rather than shear banding, as it should without the application of pulsed current. It is found that the pulsed current produces an additional effective “temperature increment” $\sim 0.15 T_g$ apart from its Joule heating effect. This expanded homogeneous regime in BMG is attributed to electromigration-induced dynamic rejuvenation, i.e. the bond-switching events⁷ created by the electric current-biased atomic diffusion^{19,20}, which promotes homogeneously distributed deformation and suppresses shear banding by enlarging the STZs.

Results

Tensile tests under pulsed electric current. Figure 1a shows a schematic illustration of the tensile test during which a pulsed electric current is applied to a Zr55 BMG specimen. Figure 1b shows the actual experimental setup, including proper modifications to enable the application of pulsed current. Figure 1c shows a close-up of the BMG specimen, the thermocouple, and the extensometer. The thermocouple monitors the real-time temperature profile of the BMG specimen under pulsed current. For the presence of pulsed current on the specimen, the circuit of the thermocouple for temperature measurement was carefully designed to avoid any possible interventions (see Supplementary

Fig. 2). Figure 1d shows the geometry of the Zr55 BMG specimen with 15 mm in gauge length and 2 mm in diameter. A specially designed power source was used to generate pulsed currents with a frequency ranging from 1 to 20 K Hz. After numerous attempts, the optimized current density is of $30\text{--}40 \text{ A}\cdot\text{mm}^{-2}$, which could avoid the crystallization of Zr55 BMG induced by Joule heating effect of the pulsed current. A square wave was adopted for the current pulses, as illustrated in Fig. 1e. Example measurements of a real pulsed current generated by our experimental apparatus are shown in Fig. 1f, with a pulse width $t_w = 0.5 \text{ ms}$ and a pulse period $t_p = 5 \text{ ms}$. See Supplementary Methods for more details.

Figure 2a shows the true stress–strain (SS) curves of the Zr55 BMG in tension under a strain rate of $2 \times 10^{-4} \text{ s}^{-1}$ and pulsed currents of different density i from 0 to $38 \text{ A}\cdot\text{mm}^{-2}$ (with a pulse width $t_w = 10 \text{ ms}$ and a pulse period $t_p = 400 \text{ ms}$). The SS curve at $i = 0 \text{ A}\cdot\text{mm}^{-2}$ was obtained by a normal tensile test without pulsed current. To clearly monitor the effect of pulsed current on the tension of Zr55 BMG, the SS curves at $i = 30\text{--}38 \text{ A}\cdot\text{mm}^{-2}$ were obtained in tensile tests during which the specimens were pre-loaded to 600 MPa prior to the application of pulsed current. Tensile tests with different pre-loads were also performed to obtain the similar results (see Supplementary Fig. 3). On the SS curves at $i = 30\text{--}38 \text{ A}\cdot\text{mm}^{-2}$, the stress drops slightly upon the application of pulsed current at 600 MPa, indicating a transient softening effect caused by pulsed current. After the slight drop, the stress increases again upon further loading. The SS curves at $i = 0 \text{ A}\cdot\text{mm}^{-2}$ and $i = 30 \text{ A}\cdot\text{mm}^{-2}$ exhibit an abrupt drop upon the yielding of Zr55 BMG, which is suggestive of a brittle fracture, i.e. an inhomogeneous deformation. However, at $i = 30 \text{ A}\cdot\text{mm}^{-2}$, the yield strength σ_y is reduced to 1260 MPa, and the Young’s modulus E is reduced to 50 GPa (from 79 GPa at $i = 0 \text{ A}\cdot\text{mm}^{-2}$); this is also indicative of the softening effect induced by pulsed current. As i is further increased to $33 \text{ A}\cdot\text{mm}^{-2}$, σ_y is reduced to 930 MPa, and E is reduced to 26 GPa, respectively. More importantly, the Zr55 BMG exhibits a homogeneous plastic strain ϵ_u of $\sim 1.5\%$ before necking starts at a peak stress $\sigma_p = 1050 \text{ MPa}$, and a total elongation ϵ_p of $\sim 16.6\%$. At $i = 35$ and $38 \text{ A}\cdot\text{mm}^{-2}$, more pronounced softening and similar elongations are observed.

The photograph of Zr55 BMG specimens tested at $i = 0 \text{ A}\cdot\text{mm}^{-2}$ and $i = 33 \text{ A}\cdot\text{mm}^{-2}$ is shown in Fig. 2b. The specimen tested at $i = 33 \text{ A}\cdot\text{mm}^{-2}$ exhibits a typical elongation followed by necking, instead of the shear banding observed on the specimen tested at $i = 0 \text{ A}\cdot\text{mm}^{-2}$. The close-up shown in Fig. 2c also indicates no sign of shear banding at $i = 33 \text{ A}\cdot\text{mm}^{-2}$ (see also Supplementary Movie 1). These results suggest an inhomogeneous-to-homogeneous transition in the deformation of Zr55 BMG with increasing current density. Supplementary Table 1 summarizes the data of the mechanical properties of Zr55 BMG under different current densities, including the yield strength σ_y and the total elongation ϵ_p .

The amorphous structure in the necking region of Zr55 BMG (Fig. 2c) after the tensile test at $i = 33 \text{ A}\cdot\text{mm}^{-2}$ was examined by high-resolution transmission electron microscopy (HRTEM). As seen in Fig. 2d, no sign of crystallization is observed. Differential scanning calorimetry and X-ray diffraction were also performed on all BMG specimens after tension (see Supplementary Fig. 4 and Supplementary Table 2); these results also indicate no obvious crystallization of the BMG specimens during the test, regardless of current density.

Evaluating the Joule heating effect. To reveal the origin of the homogeneous deformation observed in Fig. 2, we evaluated the Joule heating effect of the pulsed current. As shown in Fig. 1c, the real-time temperature profile of the BMG specimen during tensile test was monitored by a thermocouple. In addition, both thermal

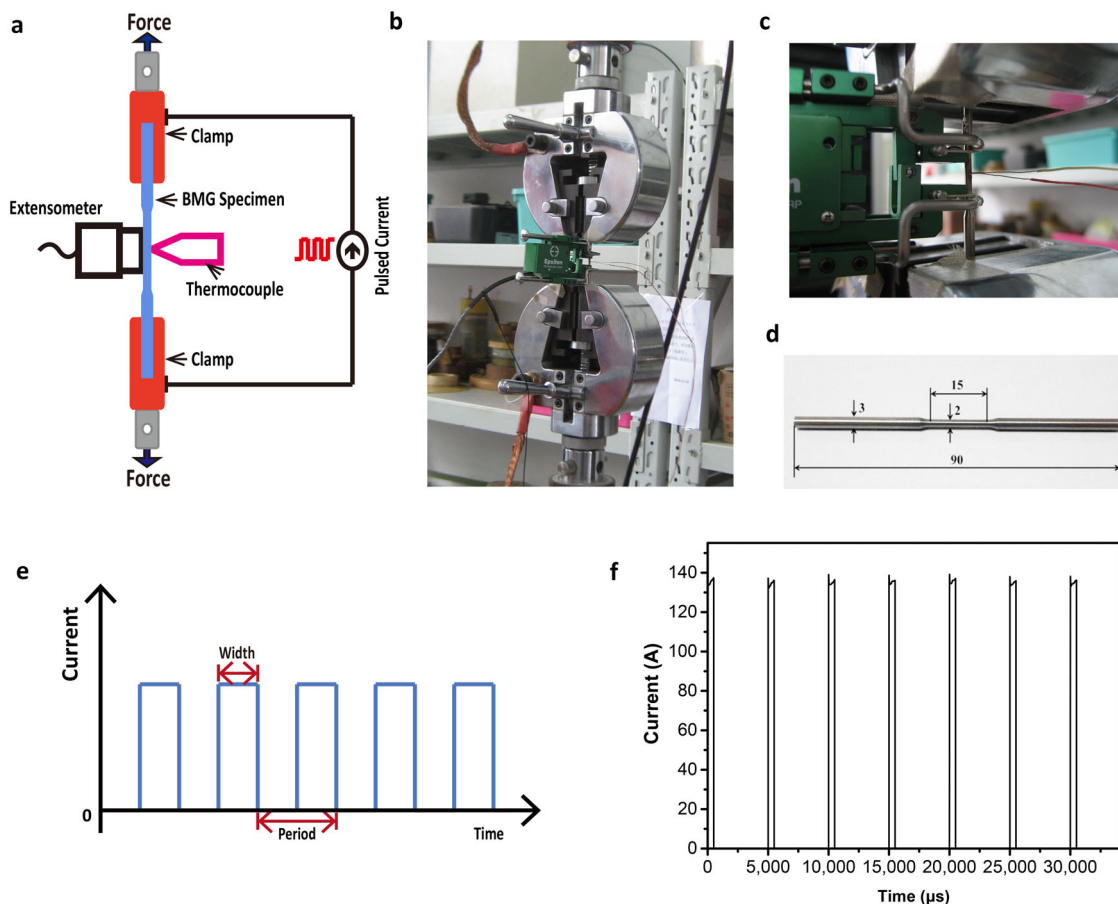


Fig. 1 The experimental scheme of tensile tests on $\text{Zr}_{55}\text{Cu}_{30}\text{Al}_{10}\text{Ni}_5$ (Zr55) bulk metallic glass (BMG) with pulsed electric current applied to the BMG specimen. **a** Schematic illustration of the experimental setup; **b** actual experimental setup, and **c** close-up on the BMG specimen, the thermocouple, and the extensometer; **d** geometry of the BMG specimen for tensile test; **e** illustration on the pattern of the current pulses adopted, a square wave; **f** an example of the current pulses actually generated, a square wave with a pulse width of 0.5 ms, and a pulse period of 5 ms.

infrared imaging and finite element simulations were leveraged to confirm the uniformity of the temperature field in the gauge portion of the specimen (see Supplementary Fig. 5 and Supplementary Movie 2). As shown in Fig. 3a, all temperature profiles of the BMG specimens initially display a linear increase at similar rates ($\sim 5.5 \text{ K}\cdot\text{s}^{-1}$) and gradually plateau after $\sim 100 \text{ s}$. The plateau temperature increases with increased current density, e.g. 523 K at $i = 30 \text{ A}\cdot\text{mm}^{-2}$, 553 K at $i = 33 \text{ A}\cdot\text{mm}^{-2}$, 603 K at $i = 35 \text{ A}\cdot\text{mm}^{-2}$, and 643 K at $i = 38 \text{ A}\cdot\text{mm}^{-2}$. The slight increase of temperature at the rear part of the profiles at $i = 33\text{--}38 \text{ A}\cdot\text{mm}^{-2}$ is probably due to a reduction in the cross-section area of the BMG specimen, which increases the electric resistance. Noted the onset temperature of glass transition for Zr55 BMG is $T_{g\text{-onset}} = 693 \text{ K}$, the highest specimen temperature is 643 K observed at $i = 38 \text{ A}\cdot\text{mm}^{-2}$, which is still 50 K below $T_{g\text{-onset}}$. Thus, the temperature profiles in Fig. 3a indicate that the homogeneous deformation observed in Fig. 2 is not due to the flow of Zr55 BMG in supercooled liquid state^{15,21}.

To examine whether the homogenous deformation was due to the temperature rise caused by Joule heating effect, tensile tests at elevated temperatures in a furnace on Zr55 BMG were also conducted. The true SS curves at 623 K ($0.89 T_g$) and 653 K ($0.94 T_g$) are shown in Fig. 3b, and the morphologies of tested specimens are shown in Fig. 3c. The specimen tested at 623 K exhibits a typical brittle failure via shear banding, in sharp contrast to the homogeneous elongation and necking of the specimen tested under $i = 33 \text{ A}\cdot\text{mm}^{-2}$ (Fig. 2b), of which the specimen temperature is merely 553 K. The unusual large elastic strain 4% is probably due to

the limited stiffness of the testing machine. At $T = 653 \text{ K}$, the Zr55 BMG starts to exhibit necking. It is also important to note that the yield strength (500 MPa) of the BMG specimen tested under $i = 38 \text{ A}\cdot\text{mm}^{-2}$, of which the specimen temperature is 643 K, is much lower than that (1.3 GPa) of the BMG specimen tested at 653 K. Therefore, these results suggest that the homogeneous deformation observed in Fig. 2 cannot be attributed to the temperature rise, and that the pulsed current has a stronger softening effect than temperature rise.

To further exclude the role of temperature rise, the effects of pulse width (t_w) and pulse period (t_p) on the tension of Zr55 BMG were examined. Pulsed currents of various t_w values (10, 40, 80, and 100 ms) with a constant ratio of $t_p/t_w = 40$ were used at a constant current density of $i = 33 \text{ A}\cdot\text{mm}^{-2}$. As seen in Fig. 4a, the true SS curves of Zr55 BMG under pulsed currents of different t_w exhibit a prominent decrease in yield strength with increasing t_w . This observation indicates the nonlinear softening effect caused by the pulsed current with increased t_w , as the total currents passing through a BMG specimen in a certain period are the same under different t_w values if the ratio t_p/t_w keeps constant. Moreover, the homogeneous deformation ϵ_u increases with t_w , e.g. from $\epsilon_u = 1.5 \%$ at $t_w = 10 \text{ ms}$ to $\epsilon_u = 2.8\%$ at $t_w = 100 \text{ ms}$.

Intriguingly, the SS curves exhibit increasing serrations as t_w is increased from 10 to 100 ms (tiny serrations can also be observed on the SS curve of $t_w = 10 \text{ ms}$. For more information on the serrations, see Supplementary Figs. 6 and 7). The temperatures of BMG specimens under different pulse widths are shown in Fig. 4b; these profiles also exhibit serrations, yet the temperatures

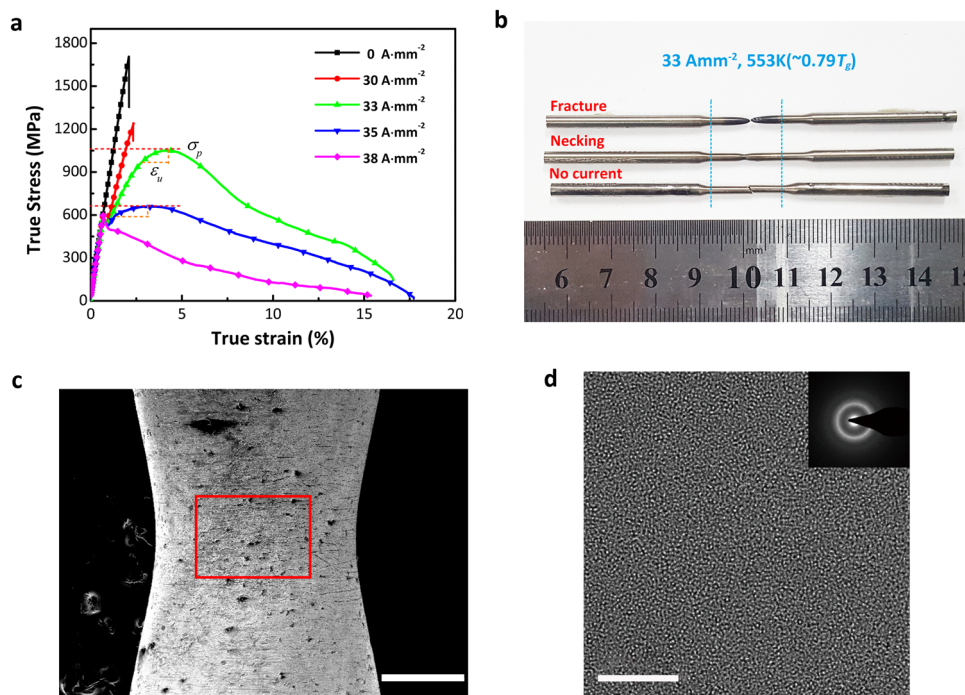


Fig. 2 Tensile tests on $\text{Zr}_{55}\text{Cu}_{30}\text{Al}_{10}\text{Ni}_5$ (Zr55) bulk metallic glass (BMG) with pulsed electric currents of different density i applied on the BMG specimen ($i = 0, 30, 33, 35,$ and $38 \text{ A}\cdot\text{mm}^{-2}$). The pulsed currents are of a constant pulse width $t_w = 10 \text{ ms}$ and a constant pulse period $t_p = 400 \text{ ms}$. **a** True stress-strain (SS) curves in tension, and **b** morphologies of the tested BMG specimens, indicating an inhomogeneous-to-homogeneous transition upon increasing current density; **c** close-up on the necking region, indicating no sign of shear banding in the BMG specimen tested at a current density of $33 \text{ A}\cdot\text{mm}^{-2}$; scale bar is $500 \mu\text{m}$. **d** High-resolution TEM images of the atoms in the necking region of the BMG specimen tested at a current density of $33 \text{ A}\cdot\text{mm}^{-2}$, from the zone indicated by the rectangle in **(c)**, demonstrating the maintained amorphous structure of Zr55 BMG after tension under pulsed current. Scale bar is 5 nm .

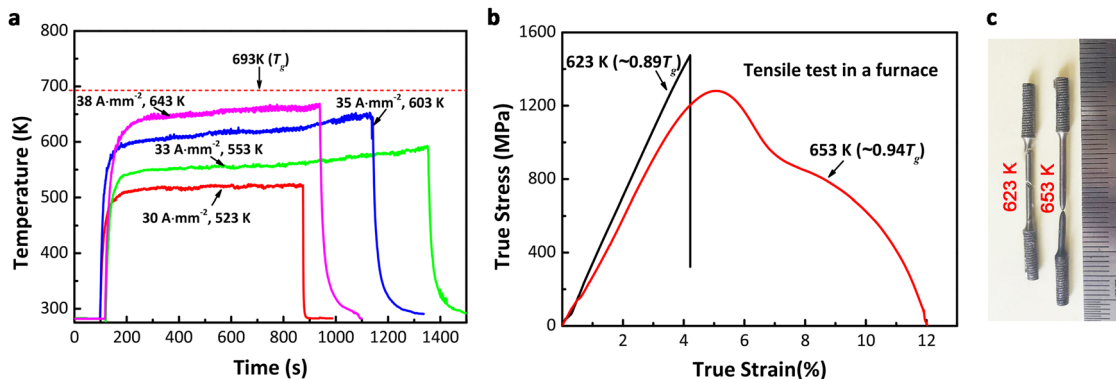


Fig. 3 Evaluation of the Joule heating effect. **a** Real-time temperature profiles of $\text{Zr}_{55}\text{Cu}_{30}\text{Al}_{10}\text{Ni}_5$ (Zr55) bulk metallic glass (BMG) specimens during tensile tests under pulsed currents of different current density, confirming that the specimen temperatures are below the glass transition temperature T_g ; **b** true stress-strain (SS) curves of Zr55 BMG in tension at elevated temperatures in a furnace under no pulsed current; **c** morphologies of Zr55 BMG specimens after tensile tests at elevated temperatures in a furnace. The specimen tested at 623 K exhibits a brittle fracture via shear banding, in contrast to the elongation and necking of the BMG specimen tested under a pulsed current of a density $i = 33 \text{ A}\cdot\text{mm}^{-2}$, of which the specimen temperature is 553 K , even 70 K lower, indicating that the homogeneous deformation of Zr55 BMG under pulsed i current is not due to the temperature rise caused by Joule heating effect. The specimen tested at 653 K exhibits necking.

remain below $T_{g\text{-onset}} = 693 \text{ K}$. To better convey the relationship between temperature rise and homogeneous deformation, the synchronized signals of stress vs. displacement and temperature vs. displacement of BMG specimen in the time domain are presented in Fig. 4c, d, respectively. Please note that the stress and temperature are derived from the SS curve and the temperature profile of $t_w = 100 \text{ ms}$, respectively. The displacement of the BMG specimen was recorded by an extensometer.

In Fig. 4c, the displacement displays a jump that accompanies a drop in the stress during the period Δt_1 , and remains nearly constant in Δt_2 even when the stress is increased continuously. The time intervals associated with the displacement jumps and the stress drops match the pulse period t_p well, indicating that the transient softening of Zr55 BMG (i.e., the displacement jump) is a consequence of current pulse exposure, and that the increased homogeneous deformation and stress serration (Fig. 4a) are

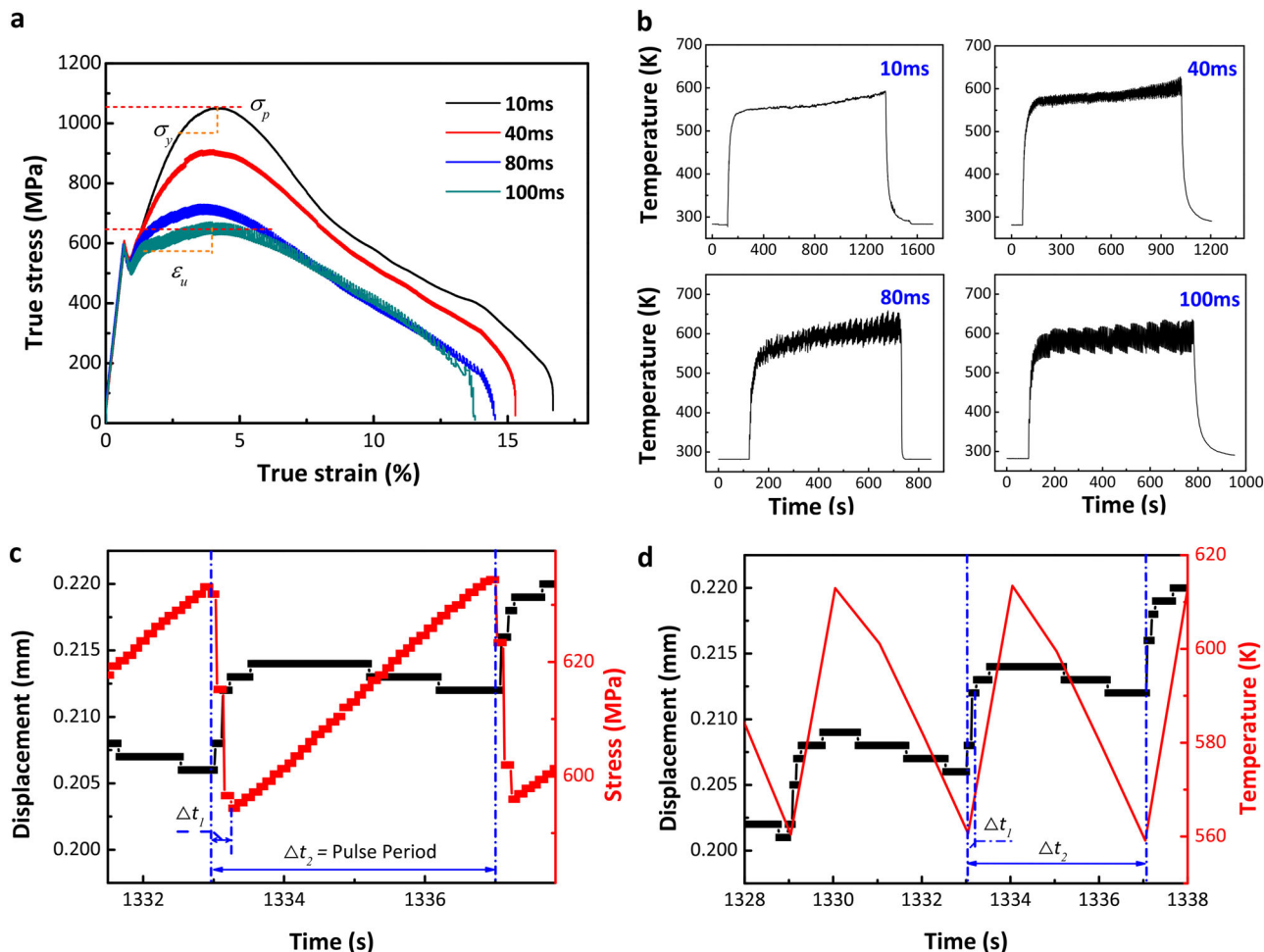


Fig. 4 Tensile tests on $\text{Zr}_{55}\text{Cu}_{30}\text{Al}_{10}\text{Ni}_5$ (Zr55) bulk metallic glass (BMG) under a strain rate of $2 \times 10^{-4} \text{ s}^{-1}$ and pulsed currents of different pulse width $t_w = 10, 40, 80,$ and 100 ms . The pulsed currents are of a constant current density $i = 33 \text{ A}\cdot\text{mm}^{-2}$ and a constant pulse width vs. pulse period ratio: $t_w/t_p = 1:40$. **a** True stress–strain (SS) curves; **b** real-time temperature profiles during tensile tests; **c** typical stress serrations from the SS curve of $t_w = 100 \text{ ms}$, and the corresponding evolution of the displacement of BMG specimen plotted in time domain, correlating well with the passing through of current pulses; **d** typical temperature serrations from the temperature profile of $t_w = 100 \text{ ms}$, and the corresponding evolution of the displacement of BMG specimen plotted in time domain. After the jump in Δt_1 , the specimen displacement does not continuously increase when the specimen temperature maintains a high value in Δt_2 , confirming that the homogeneous deformation is independent of the temperature rise.

intrinsically related to current pulses with greater t_w . In Fig. 4d, the synchronous periodic variations of temperature and displacement indicate the prompt response of the thermocouple to the current pulses. Clearly, the changes in the displacement do not follow the variation of the temperature. After the initial jump occurred during the period Δt_1 , the displacement does not increase while the elevated temperature is maintained in the earlier part of Δt_2 . This result confirms that the homogeneous deformation of Zr55 BMG is independent of the temperature rise.

The data on the mechanical properties of Zr55 BMG under various t_w values are collected in Supplementary Table 3. Supplementary Table 4 summarizes the serration data under various t_w values, including the amplitude of stress serration ($\Delta\sigma$), the maximum (T_{max}), and minimum (T_{min}) in a temperature serration, the time interval of stress drop (Δt_1), and the time interval of stress increase (Δt_2).

The above results show that homogeneous deformation was achieved in Zr55 BMG under a strain rate of $2 \times 10^{-4} \text{ s}^{-1}$ at $\sim 0.8 T_g$ (553 K) via the application of a pulsed electric current. However, the homogeneous deformation was not attributable to the Joule heating effect of the current. As shown in Fig. 3 and Supplementary Fig. 1,

for Zr55 BMG, at a strain rate of $2 \times 10^{-4} \text{ s}^{-1}$, homogeneous deformation is only accessible at temperature near and above $\sim 0.95 T_g$. Thereby, our work indicates that the homogeneous regime of deformation in the Zr55 BMG was expanded by the pulsed current, which produced an effective “temperature increment” of $\sim 0.15 T_g$. Please also note that the pulse interval during which the current is absent might have a crucial effect on the deformation of Zr55 BMG. For the lack of work-hardening mechanism in BMGs²², during the pulse interval, without the effect of electric current, the self-assembly of STZs would lead to a high level of structural inhomogeneity and softening which triggers necking. This is probably why the Zr55 BMG starts necking easily, as shown in Figs. 2a and 4a, wherein with the current density changes from 33 to $38 \text{ A}\cdot\text{mm}^{-2}$ and the pulse width from 10 to 100 ms, the homogeneous plastic deformation remain $<3\%$, while the yield strength of Zr55 BMG decreases prominently.

Discussion

The key question is: how does the electric current expand the homogenous regime of deformation in BMGs? In BMGs, the existence of free volume leads to a nonuniform packing of atoms²³. As

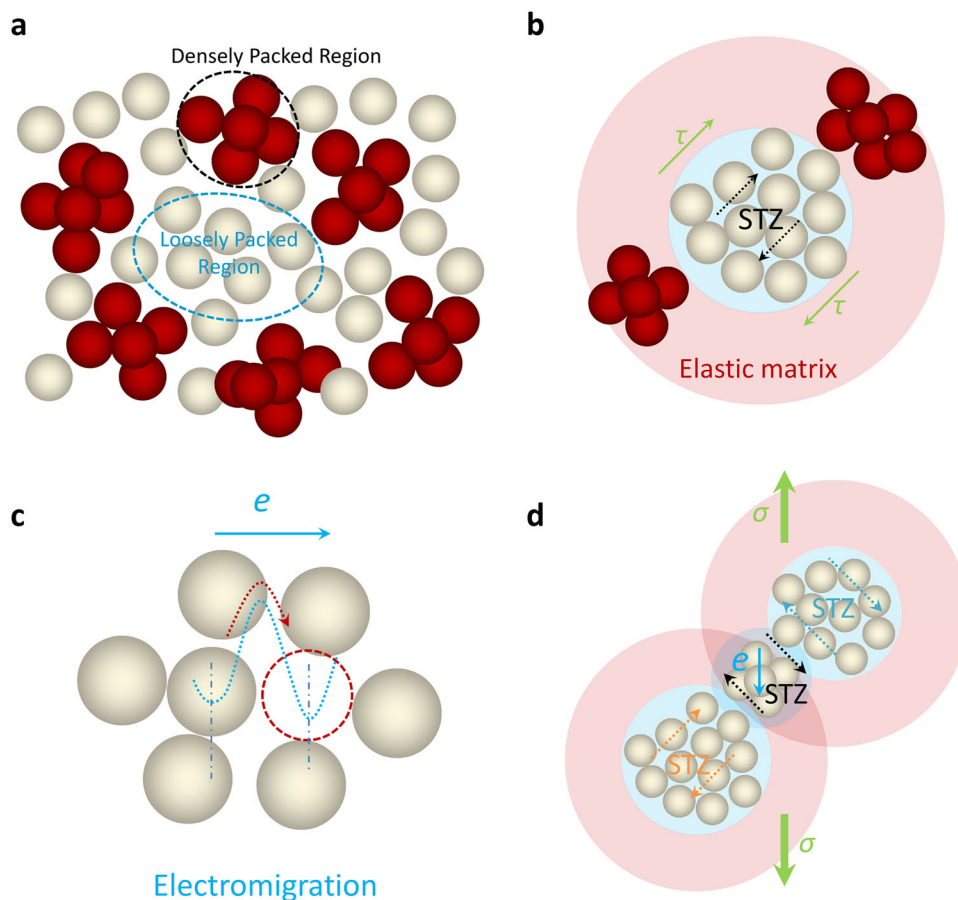


Fig. 5 Illustration on the dynamic rejuvenation of bulk metallic glasses (BMGs) driven by the electron-scattering force in electromigration. **a** Randomly distributed densely packed regions which contain less free volume (red spheres), and loosely packed regions which contain more free volume (white spheres), for the existence of free volume in BMGs. **b** Under external loading, the atoms in soft loosely packed regions develop into shear transformation zones (STZs) to carry plastic deformation by participating in shear transformation, while the atoms in strong densely packed regions act as an elastic matrix and confine the STZs. The atoms in densely packed regions do not participate in shear transformation, and do not contribute to plastic deformation. **c** Atomic diffusion promoted by the electron-scattering force along the direction of electron transport in electromigration, where the more densely packed atoms suffer a larger force. This atomic diffusion is virtually the free volume-based flow mechanism of BMGs. **d** The electron-scattering force preferentially drives the atoms in the strong densely packed regions, which confine STZs to participate in shear transformation and contribute to plastic deformation, i.e. creates bond-switching events, thus promoting homogeneously distributed deformation.

illustrated in Fig. 5a, there is a random distribution of densely packed regions containing less free volume (red spheres) and loosely packed regions containing more free volume (white spheres)²⁴. Under external loading, the loosely packed regions (soft regions) readily develop into STZs to accommodate plastic deformation²⁵, while the densely packed regions (strong regions) act as an elastic matrix confining the STZs and do not contribute to plastic deformation²², as shown in Fig. 5b. Second, it is critical to note the atomistic mechanism by which an electric current causes electromigration. When an electric current passes through a conductor, electrons scattered from the conductor atoms promote atomic diffusion in the direction of electron transport via what is referred as the electron-scattering force²⁰; this process is illustrated in Fig. 5c^{26,27}. Importantly, Bondarchuk et al.²⁸ found that geometrically constrained atoms (i.e., densely packed atoms) experience greater electron-scattering force than do more freely diffusing atoms (loosely packed atoms). In BMGs, this is because that the densely packed atoms are of more perfect icosahedral order²⁹ and thereby of higher electric resistance, leading to more momentum transferred from the electrons to these atoms, i.e. a higher electron-scattering force, as more perfect icosahedral order is of higher electric resistivity³⁰, even higher than the amorphous state.

Therefore, when the pulsed current is applied on BMG, the diffusion of densely packed atoms in the elastic matrix can be preferentially enhanced by the electron-scattering force. This enhanced atomic diffusion²⁶ functions analogously to the classical free volume-based flow mechanism in BMGs⁷, creating numerous homogeneously distributed bond-switching events. Consequently, the strong densely packed regions that confine STZs are driven to participate in shear transformation and contribute to overall plastic deformation, namely, the STZs are enlarged. Moreover, As noted by Sopy et al.¹², it is the densely packed regions that convey the long-range interactions between STZs, which lead to the self-assembly of STZs¹² into shear bands. Therefore, with the densely packed regions driven to participate in shear transformation, the long-range interactions between STZs would be relaxed and the self-assembly of STZs¹² into shear bands will be suppressed. Under these circumstances, the BMG will exhibit homogeneously distributed deformation, as illustrated in Fig. 5d. The electron-scattering force preferentially enhancing the atomic diffusion of the densely packed regions in BMG explains why the electric current has a stronger softening effect than temperature rise, as the strong densely packed regions are the origin of the strength of BMGs²⁹.

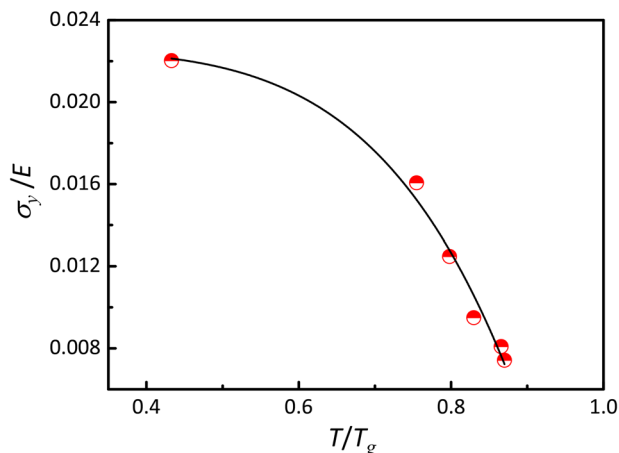


Fig. 6 The relation of specimen temperature T vs. yield strength σ_y for the $Zr_{55}Cu_{30}Al_{10}Ni_5$ (Zr55) bulk metallic glass (BMG). The data are fitted to the power law: $\sigma_y \sim (T/T_g)^n$, suggesting $n \sim 5.2$. E is the Young's modulus. T_g is the glass transition temperature.

To justify that the atomic diffusion in Zr55 BMG was enhanced by pulsed current, it is important to recall the reported atomic diffusivities³¹ (10^2 – 10^4 nm²·s⁻¹) induced by electromigration in metal conductors under current densities of $\sim 10^3$ A·mm⁻². Noting that the widely reported atomic self-diffusivity³² of BMGs at temperatures above T_g is around 10^{-4} – 10^0 nm²·s⁻¹, a current density of 30–40 A·mm⁻² should be sufficient to induce a diffusivity comparable with that of BMG above T_g (i.e., 10^{-4} – 10^0 nm²·s⁻¹). This is corroborated by the results displayed in Figs. 2a and 4a, where the softening of Zr55 BMG—as indicated by the largely reduced yield strength σ_y and Young's modulus E —is comparable with the softening of BMG at temperatures above T_g . Specifically, the Young's modulus of BMGs usually shows a very weak temperature (T) dependence³³ below T_g , i.e. $\sim 10^{-3}$ GPa·K⁻¹. However, the SS curves in Figs. 2a and 4a suggest a more significant dependence of Young's modulus on temperature: $\sim 10^{-1}$ GPa·K⁻¹, under pulsed current. Moreover, the temperature dependence of σ_y for BMGs has been formulated by Johnson & Samwer³⁴ by a power law relation: $\sigma_y \sim (T/T_g)^{2/3}$. The relation between specimen temperature T and σ_y in this work was also fitted to the power law: $\sigma_y \sim (T/T_g)^n$, and the result is provided in Fig. 6. The obtained $n \sim 5.2$ is significantly larger than $2/3$, suggesting that the pulsed current has a much stronger softening effect than is typical for thermal softening. Therefore, the softening effect shown in Figs. 2a and 4a indicates that the atomic diffusion in Zr55 BMG is substantially enhanced by electromigration.

Recently, Zheng et al.³⁵ reported that nano-sized amorphous silica exhibited superior deformability when the tensile test was performed in situ under irradiation by electron beam. The enhanced deformability of amorphous silica was attributed to irradiation-induced dynamic rejuvenation³⁶, during which the electron beam continuously stimulated bond-switching events within the disordered atomic structure of amorphous silica and promoted a homogeneously distributed flow. Thereby, we propose that the homogeneous deformation displayed by Zr55 BMG in this work is caused by the electromigration-induced dynamic rejuvenation, similar to that in amorphous silica caused by the irradiation-induced dynamic rejuvenation³⁶. We also performed normal tensile test on a post-rejuvenated Zr55 BMG specimen (rejuvenated by a pulsed current with $i = 33$ A·mm⁻², $t_w = 10$ ms, and $t_p = 400$ ms for 2 h); the BMG specimen exhibited a brittle fracture without any homogeneous plastic deformation (see Supplementary Fig. 8). This is consistent with the post-rejuvenated amorphous silica which is also brittle³⁵, suggesting that homogeneous plastic deformation originates from the

dynamic rejuvenation effect. This dynamic rejuvenation is different from the temperature-driven rejuvenation of BMG by capacitor discharging-based flash annealing technique³⁷, where the BMG was heated above T_g (to a state with much increased enthalpy) in less than a millisecond followed by subsequent freezing.

Although the dynamic rejuvenation induced by electromigration is dominating in the homogeneous deformation of Zr55 BMG, it is noted that the Joule heating effect which might as well be noncritical, yet still increases the atomic mobility and assists the deformation. The mechanical rejuvenation³⁸ induced by tensile deformation also increases the concentration of free volume and aids in the homogeneous deformation. Thereby, in total, assisted by Joule heating and mechanical rejuvenation, the electromigration-induced dynamic rejuvenation enlarges the STZs and enables homogeneously distributed deformation, thus suppressing the self-assembly of STZs into shear bands¹² in BMG.

In conclusion, the homogenous regime of deformation in the Zr55 BMG was expanded through the application of a pulsed electric current which produced an additional effective “temperature increment” $\sim 0.15 T_g$ besides its Joule heating effect. This expansion of homogenous regime is attributed to the electromigration-induced dynamic rejuvenation, where the bond-switching events created by electromigration promote homogeneous plastic deformation via enlarging STZs. However, the following issues remain to be clarified in the future, such as how electromigration alters the structure of BMG, what the mechanism of the nonlinear softening effect of electromigration is, and how to measure the relaxation time of BMG under electric current. Further studies on these issues would be of great help to understanding the origin of plasticity in glassy materials.

Methods

Sample preparation. Alloy ingots with a nominal composition of $Zr_{55}Cu_{30}Al_{10}Ni_5$ BMG were prepared from elemental metals (purity > 99.5%) by arc melting under a Ti-gettered argon atmosphere. From the master alloy, rods of 3 mm in diameter and of 90 mm in length were fabricated by copper-mold suction casting. Specimens of 15 mm in gauge length and of 2 mm in gauge diameter for uniaxial tensile tests were prepared by carefully machining from the as-cast rods (Fig. 1d). To remove any possible structure differences in the fabricated BMG rods between different batches, all specimens were annealed at 663 K ($\sim 0.95 T_g$, where $T_g = 693$ K is the onset temperature of glass transition) for 2 h under vacuum prior to uniaxial tension.

Tensile test. Tensile tests on the BMG specimens were carried out with an electro-mechanical testing machine, Reger RGM-4100, under a constant quasi-static strain rate of 2×10^{-4} s⁻¹. The pulsed electric current applied to the BMG specimens was generated by a specially designed, in-house produced electric power source featuring a programmable pulse controller. The experimental setup is shown in Fig. 1a, b. In order to accurately monitor the temperature of the BMG specimen during the tensile tests, an Omega-TT-K-30-SLE thermocouple was welded onto the surface of each BMG specimen. An extensometer with a gauge length of 10 mm was affixed to the BMG specimens for accurate recording of deformations. Reference tensile tests—at elevated temperatures and without pulsed current—were also carried out at the same strain rate 2×10^{-4} s⁻¹ on a material-testing machine, MTS CMT5105S, equipped with a high-temperature furnace. The temperature control resolution of the furnace is ± 1 K. It is necessary to point out that, to accurately evaluate the effect of pulsed current, particular cautions should be taken in measuring the responses of BMG specimens to external load under pulsed current, as the function of the sensors detecting the responses of BMG specimens is mostly based on electric signals. It is crucial to avoid any potential interventions between the pulsed current and the circuits of the sensors. More details on the equipment used during this work can be found in Supplementary Methods.

Structure analysis. The amorphous structure of the as-annealed BMG rods and the deformed BMG specimens were examined via X-ray diffraction under Cu K α radiation (Philips, X'Pert Pro). The samples for XRD investigation were taken from the adjacent part near the necking region. The thermal properties of the BMG specimens—both before and after tensile tests—were characterized with a differential scanning calorimeter (Perkin Elmer DSC 7) at a heating rate of 20 K/min under a constant flow of high-purity argon. High-resolution transmission electron

microscopy (HRTEM) images of each specimen after tensile tests were acquired with a Tecnai G2 F20 TEM system.

Data availability

The authors declare that the data supporting the findings contained within this study will be made available from the corresponding authors upon request.

Received: 4 October 2019; Accepted: 13 June 2020;

Published online: 17 July 2020

References

- Nabarro, F. R. N. Dislocations in a simple cubic lattice. *Proc. Phys. Soc.* **59**, 256 (1947).
- Wang, Y. M. et al. Defective twin boundaries in nanotwinned metals. *Nat. Mater.* **12**, 697–702 (2013).
- Shan, Z. W. et al. Grain boundary-mediated plasticity in nanocrystalline nickel. *Science* **305**, 654–657 (2004).
- Nicolas, A., Ferrero, E. E., Martens, K. & Barrat, J. L. Deformation and flow of amorphous solids: insights from elastoplastic models. *Rev. Mod. Phys.* **90**, 63 (2018).
- Ashby, M. F. A first report on deformation-mechanism maps. *Acta Metallurgica* **20**, 887–897 (1972).
- Frost, H. J. & Ashby, M. F. *Deformation-Mechanism Maps: The Plasticity and Creep of Metals and Ceramics* (Pergamon Press, 1982).
- Spaepen, F. A microscopic mechanism for steady state inhomogeneous flow in metallic glasses. *Acta Metallurgica* **25**, 407–415 (1977).
- Schuh, C. A., Hufnagel, T. & Ramamurty, U. Mechanical behavior of amorphous alloys. *Acta Mater.* **55**, 4067–4109 (2007).
- Lu, J., Ravichandran, G. & Johnson, W. L. Deformation behavior of the $Zr_{41.2}Ti_{13.8}Cu_{12.5}Ni_{10}Be_{22.5}$ bulk metallic glass over a wide range of strain-rates and temperatures. *Acta Mater.* **51**, 3429–3443 (2003).
- Liu, Y. H. et al. Super plastic bulk metallic glasses at room temperature. *Science* **315**, 1385–1388 (2007).
- Greer, A. L., Cheng, Y. Q. & Ma, E. Shear bands in metallic glasses. *Mater. Sci. Eng. R-Rep* **74**, 71–132 (2013).
- Sopu, D., Stukowski, A., Stoica, M. & Scudino, S. Atomic-level processes of shear band nucleation in metallic glasses. *Phys. Rev. Lett.* **119**, 195503 (2017).
- Falk, M. L. & Langer, J. S. Dynamics of viscoplastic deformation in amorphous solids. *Phys. Rev. E* **57**, 7192–7205 (1998).
- Hufnagel, T. C., Schuh, C. A. & Falk, M. L. Deformation of metallic glasses: recent developments in theory, simulations, and experiments. *Acta Mater.* **109**, 375–393 (2016).
- Nieh, T. G. & Wadsworth, J. Homogeneous deformation of bulk metallic glasses. *Scr. Mater.* **54**, 387–392 (2006).
- Johnson, W. L., Lu, J. & Demetriou, M. D. Deformation and flow in bulk metallic glasses and deeply undercooled glass forming liquids—a self consistent dynamic free volume model. *Intermetallics* **10**, 1039–1046 (2002).
- Falk, M. L., Langer, J. S. & Pechenik, L. Thermal effects in the shear-transformation-zone theory of amorphous plasticity: comparisons to metallic glass data. *Phys. Rev. E* **70**, 011507 (2004).
- Ekambaram, R., Thamburaja, P. & Nikabdullah, N. On the evolution of free volume during the deformation of metallic glasses at high homologous temperatures. *Mech. Mater.* **40**, 487–506 (2008).
- Tan, C. M. & Roy, A. Electromigration in ULSI interconnects. *Mater. Sci. Eng. R-Rep* **58**, 3–75 (2007).
- Tao, C. G., Cullen, W. G. & Williams, E. D. Visualizing the electron scattering force in nanostructures. *Science* **328**, 736–740 (2010).
- Reger-Leonhard, A., Heilmair, M. & Eckert, J. Newtonian flow of $Zr_{55}Cu_{30}Al_{10}Ni_5$ bulk metallic glassy alloys. *Scr. Mater.* **43**, 459–464 (2000).
- Argon, A. S. Plastic deformation in metallic glasses. *Acta Metallurgica* **27**, 47–58 (1979).
- Cohen, M. H. & Grest, G. S. Liquid-glass transition, a free-volume approach. *Phys. Rev. B* **20**, 1077–1098 (1979).
- Liu, Y. H. et al. Characterization of nanoscale mechanical heterogeneity in a metallic glass by dynamic force microscopy. *Phys. Rev. Lett.* **106**, 125504 (2011).
- Ye, J. C., Lu, J., Liu, C. T., Wang, Q. & Yang, Y. Atomistic free-volume zones and inelastic deformation of metallic glasses. *Nat. Mater.* **9**, 619–623 (2010).
- Tu, K. N. Electromigration in stressed thin films. *Phys. Rev. B* **45**, 1409–1413 (1992).
- Tu, K. N. Recent advances on electromigration in very-large-scale-integration of interconnects. *J. Appl. Phys.* **94**, 5451–5473 (2003).
- Bondarchuk, O. et al. Biased surface fluctuations due to current stress. *Phys. Rev. Lett.* **99**, 4 (2007).
- Ding, J., Cheng, Y.-Q. & Ma, E. Full icosahedra dominate local order in $Cu_{64}Zr_{34}$ metallic glass and supercooled liquid. *Acta Mater.* **69**, 343–354 (2014).
- Klein, T., Berger, C., Mayou, D. & Cyrot-Lackmann, F. Proximity of a metal-insulator transition in icosahedral phases of high structural quality. *Phys. Rev. Lett.* **66**, 2907–2910 (1991).
- Chen, K. C., Wu, W. W., Liao, C. N., Chen, L. J. & Tu, K. N. Observation of atomic diffusion at twin-modified grain boundaries in copper. *Science* **321**, 1066–1069 (2008).
- Faupel, F. et al. Diffusion in metallic glasses and supercooled melts. *Rev. Mod. Phys.* **75**, 237–280 (2003).
- Wang, W. H. The elastic properties, elastic models and elastic perspectives of metallic glasses. *Prog. Mater. Sci.* **57**, 487–656 (2012).
- Johnson, W. L. & Samwer, K. A universal criterion for plastic yielding of metallic glasses with a $(T/T_g)^{2/3}$ temperature dependence. *Phys. Rev. Lett.* **95**, 195501 (2005).
- Zheng, K. et al. Electron-beam-assisted superplastic shaping of nanoscale amorphous silica. *Nat. Commun.* **1**, 24 (2010).
- Fan, Z., Ding, J. & Ma, E. Making glassy solids ductile at room temperature by imparting flexibility into their amorphous structure. *Mater. Res. Lett.* **6**, 570–583 (2018).
- Kuchemann, S. et al. Energy storage in metallic glasses via flash annealing. *Adv. Funct. Mater.* **28**, 9 (2018).
- Zhang, M. et al. Mechanical relaxation-to-rejuvenation transition in a Zr-based bulk metallic glass. *Sci. Rep.* **7**, 625 (2017).

Acknowledgements

This work was financially supported by the National Natural Science Foundation of China under the project code Grant Nos. 51871101, 51871102, 51531003, and 51701082, and the Fundamental Research Funds for the Central Universities (HUST2015QN021). The Project was also supported by State Key Laboratory of Materials Processing and Die & Mould Technology, Huazhong University of Science and Technology. The authors are grateful to the Analytical and Testing Center, Huazhong University of Science and Technology for technical assistance.

Author contributions

Q.C. and J.C.G. performed the experimental tests; Q.C., M.Z., W.H.W., and L. Liu analyzed the data and wrote the paper; X.T.H. and L. Li designed and assembled the setup of pulsed electric current system; Q.L.C. carried out the FEM simulations; C.Z. performed the microstructure examinations; L. Liu supervised the project. All authors discussed the results and reviewed the paper.

Competing interests

The authors declare no competing interests.

Additional information

Supplementary information is available for this paper at <https://doi.org/10.1038/s43246-020-0046-x>.

Correspondence and requests for materials should be addressed to X.H., W.W. or L.L.

Reprints and permission information is available at <http://www.nature.com/reprints>

Publisher's note Springer Nature remains neutral with regard to jurisdictional claims in published maps and institutional affiliations.



Open Access This article is licensed under a Creative Commons Attribution 4.0 International License, which permits use, sharing, adaptation, distribution and reproduction in any medium or format, as long as you give appropriate credit to the original author(s) and the source, provide a link to the Creative Commons license, and indicate if changes were made. The images or other third party material in this article are included in the article's Creative Commons license, unless indicated otherwise in a credit line to the material. If material is not included in the article's Creative Commons license and your intended use is not permitted by statutory regulation or exceeds the permitted use, you will need to obtain permission directly from the copyright holder. To view a copy of this license, visit <http://creativecommons.org/licenses/by/4.0/>.

© The Author(s) 2020